Materialia 20 (2021) 101226

Contents lists available at ScienceDirect

Materialia

journal homepage: www.elsevier.com/locate/mtla

Full Length Article

Toward an energy-efficient synthesis method to improve persistent luminescence of $Sr_2MgSi_2O_7$:Eu^{2+},Dy^{3+} materials

L.G. Merízio[a,b,*], E. Bonturim[b,c], R.U. Ichikawa[d], I.G.N. Silva[e], V.C. Teixeira[f], L.C.V. Rodrigues[b], H.F. Brito[b]

[a] São Carlos Institute of Physics, University of São Paulo (IFSC – USP), São Carlos, SP 13560-970, Brazil
[b] Department of Fundamental Chemistry, Institute of Chemistry, University of São Paulo (IQ – USP), São Paulo, SP 05508-000, Brazil
[c] Department of Chemistry, School of Engineering, Mackenzie Presbyterian University, São Paulo, SP 01302-907, Brazil
[d] Nuclear and Energy Research Institute (IPEN/CNEN-SP), São Paulo, SP 05508-000, Brazil
[e] Institute of Physics, University of São Paulo (IF – USP), São Paulo, SP 05508-090, Brazil
[f] Brazilian Synchrotron Light Laboratory, Brazilian Center for Research in Energy and Materials (LNLS – CNPEM), Campinas, SP 13084-971, Brazil

ARTICLE INFO

Keywords:
Microwave-assisted solid-state synthesis
Rapid thermal annealing
Solid state reaction
Rare-earth
Luminescence
Synchrotron radiation

ABSTRACT

The synthesis of persistent luminescent materials usually requires a multi-step long time annealing at high temperatures (>1200°C) in a resistive oven, causing a huge energy consumption. Also, to achieve reduced oxidation states of emitter ions (e.g., $Eu^{3+} \rightarrow Eu^{2+}$), the H_2(g) atmosphere is often used, which can be dangerous and increase the costs of the process. Therefore, the development of a quick and new single-step green strategy, using *in-situ* low-risk atmosphere (e.g., CO(g)) and a microwave-assisted solid-state (MASS) method has been encouraged. In this work, we present a single-step method to synthesize the compound $Sr_2MgSi_2O_7$:Eu^{2+},Dy^{3+} using the MASS method and the results were compared with those prepared by a conventional ceramic method. The luminescent material was prepared in 25 min of synthesis using carbon as a microwave susceptor and CO(g) atmosphere source at the same time. A higher concentration of Eu^{2+} emitter was identified by XANES in the MASS method product, which has a significant effect on the luminescence efficiency, as well as an improvement in the optical properties, leading to an emission 100 times more intense. Furthermore, to understand the Eu^{3+} reduction process under CO(g) atmosphere, we present here the innovative results of *in-situ* XANES analysis for the $Sr_2MgSi_2O_7$:Eu^{2+},Dy^{3+} material. Finally, the MASS method makes it possible to prepare the materials with less than 5% of the ceramic method's duration in time. The energy-saving and better-quality persistent luminescent properties obtained in the MASS method provide viable applications on anti-counterfeiting markers, solar cell sensitizers, and other luminescent technologies.

1. Introduction

Global energy consumption has been increased in the last decades, mostly due to progressive technological developments. As a reflex, humanity has increasingly intensified its efforts to supply this energetic demand. However, global energy production is limited and, sometimes, costs a considerable part of the natural environment. In this context, the green chemistry principles that aim for sustainable approaches, assume the pivotal point in contemporary science. Taking the cited limitations into account, the development of efficient energy-saving methodologies, such as microwave-assisted solid-state (MASS) synthesis, deserves special attention. Recent researches point to a great improvement of functional applied compounds, owing to microwaves electromagnetic field interactions. Recently, a notable progressive optimization of persistent luminescent materials has been reported, however, the full understanding of microwave interaction remains unknown [1,2].

Persistent luminescent compounds are among the most promising candidates for applications in the lighting conversion and energy storage field. The singular capacity of emitting light for several hours (>24 h) after ceasing an irradiation source has been placed in these compounds in a prominent position [3–10]. The discovery of this class of functional materials has opened possibilities in several application areas such as anti-counterfeiting markers, emergency signs, luminescent paints, radiation detectors, solar cell sensitizers, LED devices, and more recently in biomedical diagnostics [2,7,11–15].

Generally, persistent luminescent materials consist of wide bandgap energy (E_g) inorganic host matrices, usually doped with divalent and trivalent activator ions such as Eu^{2+}, Pr^{3+}, Eu^{3+}, Tb^{3+}, Cr^{3+} or Ti^{3+}

* Corresponding author at: São Carlos Institute of Physics, University of São Paulo (IFSC – USP), São Carlos, SP 13560-970, Brazil.
E-mail address: lmerizio@ifsc.usp.br (L.G. Merízio).

https://doi.org/10.1016/j.mtla.2021.101226
Received 4 July 2021; Accepted 12 September 2021
Available online 15 September 2021

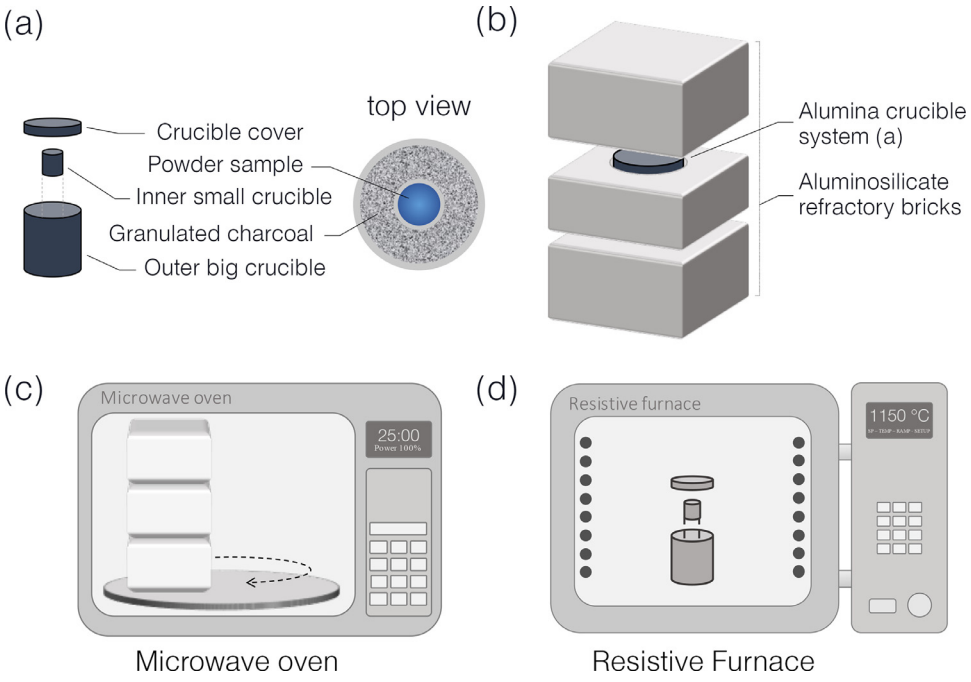

Fig. 1. Schematic representation of (a) the crucible setup, (b) the thermal insulator, (c) the microwave oven, and (d) the resistive furnace used during the syntheses [12,14].

[2,4–9,15–19]. In particular, the spectroscopic features of Eu^{2+} ion are governed by the 4f-5d interconfigurational transitions, which are strongly dependent on the lattice host ligand field. This optical property allows the modulation of the Eu^{2+} ion luminescent emission from near-infrared (NIR) to ultraviolet (UV) by using different hosts. $Sr_2MgSi_2O_7$:Eu^{2+},Dy^{3+} is a promising compound that exhibits a high persistent luminescence emission intensity in the blue region ($\lambda_{em.}$: 470 nm). The chemical and structural stabilities under high humidity and high temperatures are considered attractive features to produce multifunctional materials for applications under extreme conditions, such as the mentioned ones. Besides, the blue persistent luminescence emission of this material presents a super long time duration (>24 h), which potentializes its application possibilities [4,20,21].

The long emission time of persistent luminescence materials depends on the energy storage in electron traps, *i.e.* positive ions (*e.g.* Dy^{3+}) or even lattice defects, most commonly formed by oxygen vacancies ($V_O^{\bullet\bullet}$). The $Sr_2MgSi_2O_7$:Eu^{2+},Dy^{3+} persistent luminescence mechanism can be described as following: (*i*) the excitation energy can promote an electron from the $4f^7(^8S_{7/2})$ ground state to $4f^65d^1$ excited states of the Eu^{2+} ion; (*ii*) the electron is transferred to the conduction band (CB) followed by its storage in electron traps (Dy^{3+} ions or $V_O^{\bullet\bullet}$); (*iii*) absorbing thermal energy, the electron can return to the CB, thus recombining with Eu^{2+} excited $4f^65d^1$ levels; (*iv*) lastly, the electron radiative decays to the ground state $4f^7(^8S_{7/2})$ of the activator ion leads to the emission of light [12,17,22,23].

Despite the great potential of the disilicate materials, the most common preparation method involves high temperatures (>1100°C) combined with several hours of annealing (>5 h) and H_2 reducing atmosphere, which can represent explosion risks. This synthesis frequently uses low-efficient resistive ovens, increasing the cost and the time of its production. Therefore, new preparation methods are necessary to improve luminescent characteristics and reduce the long annealing time and high energy consumption required[14].

In this context, the microwave-assisted solid-state method (MASS) is an attractive preparation methodology to quickly obtain polycrystalline solid materials. The MASS method uses microwave electromagnetic radiation to create rapid volumetric heating, resulting in short processing times (up to 30 min) and low energy consumption compared with resistive heating methods [14,24–26]. Equipment costs and accessibility are also advantages since it is possible to use a conventional domestic microwave oven. However, microwave radiation interacts with most of the precursor samples only at high temperatures [24,25]. Therefore, it is necessary to use susceptor materials (*e.g.,* SiC, CuO, Fe_2O_3, and activated charcoal), which can absorb the microwave electromagnetic radiation and convert it to thermal energy. The use of activated charcoal as a susceptor is particularly interesting due to its high heating efficiency and the possibility to generate an *in-situ* reducing CO(g) atmosphere, which, in this case, is responsible for the reduction process of $Eu^{3+} \rightarrow Eu^{2+}$ necessary to the desired luminescent phenomenon.

In this work, we developed a single-step energy-saving synthesis of persistent luminescence $Sr_2MgSi_2O_7$:Eu^{2+},Dy^{3+} material using the microwave-assisted solid-state (MASS) method. The material was also prepared by the conventional ceramic method for comparison of structural, electronic and optical properties. In order to understand the role of the MASS preparation method, the materials were fully characterized.

Besides, to comprehend the $Eu^{3+} \rightarrow Eu^{2+}$ reduction process under CO atmosphere, we present here the first results of *in-situ* X-ray absorption spectroscopy in the XANES region for $Sr_2MgSi_2O_7$:Eu^{2+},Dy^{3+} material. This study gives important insights on the dynamics of the formation of the materials using resistive heating and, indirect understand the influence of microwave radiation in the synthesis.

2. Experimental

2.1. Material synthesis

The persistent luminescence $Sr_{1.98}MgSi_2O_7$:$0.01Eu^{2+}$,$0.01Dy^{3+}$ material was prepared *via* the microwave-assisted solid-state (MASS) and conventional ceramic methods. The material synthesized by the MASS method was obtained using $SrCO_3$ (Synth, 99.9 %), $(MgCO_3)_4Mg(OH)_2{\bullet}5H_2O$ (Sigma-Aldrich, 99.99 %), fumed SiO_2 (Sigma-Aldrich, 99.8 %), Eu_2O_3 and Dy_2O_3 (CSTARM, 99.99 %) as starting reagents. These reagents were mixed in an alumina mortar with acetone to aid the homogenization, obtaining a powder mixture called raw precursor. Then, 0.5 g of the precursor mixture was placed into a 3 mL alumina crucible. The sample crucible was positioned into a 50 mL alumina crucible containing 10 g of granular activated charcoal (Fig. 1a) partially covered to create a local reducing atmosphere of CO(g), to pro-

mote the conversion of Eu^{3+} to Eu^{2+}. The system was surrounded by aluminosilicate thermal insulation to protect the oven (Fig. 1b) of high temperature (~1350°C Supplementary Material (SM) Fig. S1) achieved in this process. Finally, the precursors were heated in a domestic microwave oven (Electrolux MEF41, 1000 W maximum power and 30 L of volume) (Fig. 1c) in a single-step synthesis for 15 min at 1000 W immediately followed by 10 min at 900 W.

In the ceramic method's preparation, 0.5 g of the raw precursor – as prepared in the MASS method – was placed in a 3 mL alumina crucible then pre-calcined in an EDG-7000 resistive furnace at 750°C for 2 h under static air atmosphere (Fig. 1d). The sample was homogenized in alumina mortar and then placed in a similar charcoal-filled alumina crucible arrangement previously described (Fig. 1a). Finally, the system was calcined at 1150°C for 5 h. The heating programs used in MASS and ceramic methods are detailed in SM Fig. S1. In order to compare the photoluminescence properties, the $Sr_2MgSi_2O_7$:Eu^{2+},Dy^{3+} commercial sample (Yada Luminescent Co. Ltd., YD-#7506) was used as a benchmark in the photoluminescence analysis.

2.2. Characterization

The thermal behavior of the physical mixture precursors used in ceramic and MASS methods was investigated with TG/DTG and DTA analyses simultaneously in a Netzsch STA 449 F1 Jupiter equipment by heating *ca.* 10 mg of each material in an aluminum oxide sample cup using an identical empty cup as reference. The solid samples were heated up to 1150°C in a 10°C min^{-1} heating rate under 50 mL min^{-1} CO(g) (or synthetic air) atmosphere.

The infrared absorption spectra (FTIR) were recorded with an FTIR PerkinElmer Frontier instrument in the spectral range of 400 to 2500 cm^{-1} with a resolution of 4.0 cm^{-1}. The powder samples were dispersed into KBr pellets and measured collecting 32 scans each in transmission mode.

The diffraction profiles were measured using synchrotron radiation X-ray powder diffraction (SR-XPD) at the XRD1 beamline of the Brazilian Synchrotron Light Laboratory, Brazilian Center for Research in Energy and Materials, (LNLS–CNPEM), Campinas–SP, Brazil [27,28]. The data were collected using Debye-Scherrer geometry and photon energy of 12 keV with a 2θ range from 3 to 120°. The detector system used was a Mythen 24 k.

Rietveld analysis was performed considering the nominal $Sr_{1.98}MgSi_2O_7$:$0.01Eu^{2+}$,$0.01Dy^{3+}$ composition through TOPAS v.6 software. SRM Si 640d from NIST was refined beforehand for 1.033155(1) Å wavelength and zero-point determination to be used in the refinements. The refined parameters were the scale factor, background coefficients (10th polynomial), lattice parameters, atomic positions, global atomic displacement factors, and occupancy for Sr^{2+} and O^{2-} ions using the modified Thompson-Cox-Hastings as a profile function. The CIF files used as starting models were $Sr_2MgSi_2O_7$ (ICSD No. 261226) and $SrSiO_3$ (ICSD No. 59308) for the materials prepared by both methods. Besides, for the material prepared by the ceramic method, $Sr_3MgSi_2O_8$ (ICSD No. 173780) was also considered.

The particle size distribution was investigated by nanoparticle tracking analysis (NTA) in a NanoSight NS300 (Malvern) equipment available at the Mass Spectrometry Laboratory from the Brazilian Biosciences National Laboratory (LNBio – CNPEM) using a 532 nm (green) laser source and an sCMOS sensor to detect the Brownian motion of the particles. The solid samples were prepared by dispersing 50 mg of the powdered sample in 2 mL distilled water at room temperature and sonicated for 1 min. The dispersion was then diluted by a factor of 1000, once again sonicated for 1 min, and then collected using a syringe pump in a continuous flow into the sample holder of the optical system. The analyses were recorded using 25 FPS (frames per second), totalizing 5 videos of 1 min for each sample [29].

The scanning electron microscopy (SEM) images were registered using a Jeol JSM-6510 equipment of the Materials Engineering Department of Mackenzie Presbyterian University (campus Higienópolis – São Paulo-SP). The samples were prepared by dispersing the powder materials in isopropanol subsequently submitted to ultrasound for 10 min. Then, 1 mL of the dispersion was deposited in a carbon stub cylinder (1 × 1 cm), which was recovered with a gold layer using a sputtering. The images were obtained in secondary electron mode (SEI) with 30 kV acceleration voltage and 10 mm of work distance (WD).

The synchrotron radiation X-ray absorption spectroscopy (XAS) was studied at the XAFS2 beamline at LNLS – CNPEM [30]. The X-ray Absorption Near-Edge Structure (XANES) measurements of the Eu element were recorded at room temperature in the fluorescence mode around the Eu-L_{III} edge, aligned using Fe (7112 eV) and Eu_2O_3 (6984 eV) as references. The beamline is equipped with a Si (111) double crystal monochromator and a 15-element Ge solid-state detector (SSD), resulting in 1.7×10^{-4} ($\Delta E/E$) energy resolution in the measured range (from -100 to 100 eV of L_{III} Fe absorption edge) [30].

The $Eu^{3+} \rightarrow Eu^{2+}$ reduction process in the synthesis was studied through the *in-situ* XANES analysis. The sample was prepared using $SrCO_3$, $(MgCO_3)_4Mg(OH)_2 \cdot 5H_2O$, fumed SiO_2, and Eu_2O_3 as starting reagents and considering 10% of europium as dopant, meaning $Sr_{1.8}MgSi_2O_7$:$0.2Eu^{2+}$. These reagents were mixed as described before and the obtained powder was pre-calcined at 750°C for 2 h in a static air atmosphere. The measurements were recorded at the DXAS beamline [31] (LNLS – CNPEM) by heating the sample from room temperature up to 1150°C under 100 mL min^{-1} He:CO (95:5 %) atmosphere. The spectra were collected in the transmission mode using a Princeton Instruments PyLon2048F CCD detector around the Eu^{3+} L_{III} edge, which was aligned in 6984 eV that is in agreement with the measurements performed at the XAFS2 beamline.

The vacuum ultraviolet-ultraviolet (VUV)–UV excitation spectra were recorded at room temperature from 4.2 to 8.2 eV, using a special quartz slide (200 mm thick), with an 8.2 eV cut off to avoid the second-order harmonics that come from the TGM beamline (LNLS – CNPEM) [32,33]. The total emission signal was collected using an SR-UV-Vis optical fiber (Ocean Optics) connected to an R928 photomultiplier (Hamamatsu) and corrected using sodium salicylate (Synth) as the standard Ref. [34]. A low-pass filter of 305 nm was used in front of the photomultiplier as an emission filter. The resolution in energy is $\Delta E/E = 700$, meaning 0.1 eV in the measured region [33,35].

The photoluminescence and persistent luminescence spectra were measured on a Horiba Jobin Yvon Fluorolog 3 spectrofluorometer equipped with mono- and double-grating monochromator (focal lengths of 0.3 and 0.5 m, respectively) for excitation and emission (iHR320), respectively. An OSRAM short-arc xenon lamp (450 W) was used as the irradiation source, and a Synapse Horiba Jobin Yvon E2 V CCD30 (1024 × 256 pixels) was used as the detector. Persistent luminescence decay curves were recorded on a SPEX Fluorolog-2 spectrofluorometer equipped with two 0.22 m SPEX1680 double-grating monochromators, a 450 W xenon lamp as the irradiation source, and photomultiplier detector. All data were collected using the equipment set up at an angle of 22.5° (front face).

The thermoluminescence (TL) measurements were carried out using a Risø TL/OSL-DA-20 luminescence reader (Institute of Physics, University of São Paulo). The TL curves were recorded from 25 to 500°C, with a 5°C s^{-1} heating rate. The same amount of sample was added to a 9.7 mm diameter stainless steel plate for all the measurements. Each sample was irradiated for 3 min using a 6 W Cole Parmer UV lamp (λ = 365 nm) with a delay of 3 min before starting the measurements.

3. Results and discussion

3.1. Thermal behavior and structural investigation

To understand the decomposition dynamics of the "raw precursor" used in the synthesis of materials it was carried out TG/DTG and DTA analyses under air atmosphere (SM Fig. S2). These thermal data indicate

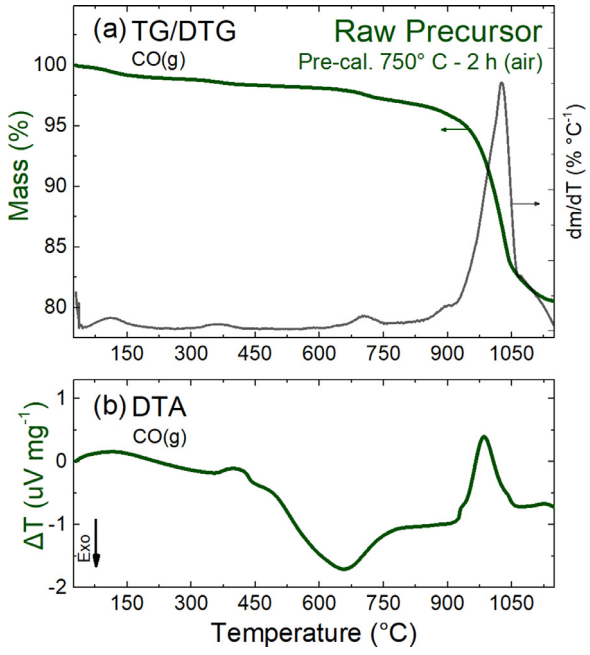

Fig. 2. (a) TG/DTG and (b) DTA curves of the raw precursors (after pre-calcination) recorded at CO atmosphere (50 mL min^{-1}) and 10°C min^{-1} heating rate.

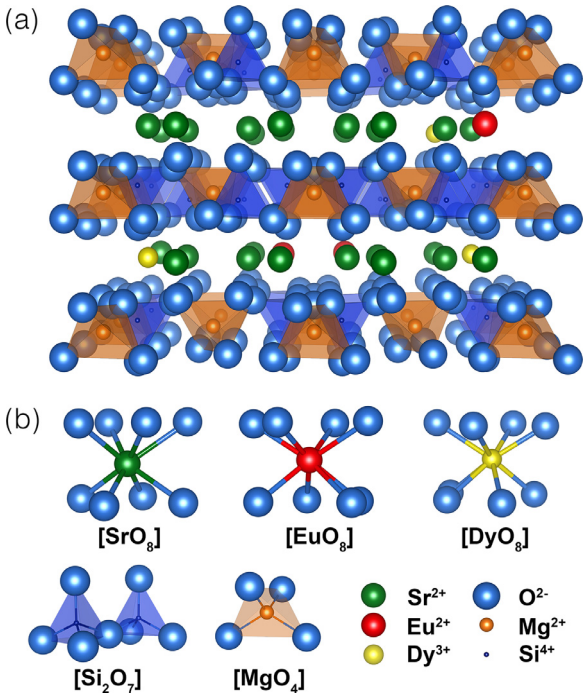

Fig. 3. (a) Crystal structure of $Sr_2MgSi_2O_7:Eu^{2+},Dy^{3+}$ in the perpendicular view from the (100) plane and (b) isolated [(Sr,Eu,Dy)O_8], [Si_2O_7] and [MgO_4] units designed on VESTA software [41] using PDF 01-075-1736 Ref.[40].

the releasing of $H_2O(g)$ and $CO_2(g)$ molecules as described in the SM Table S1 [36]. Therefore, to simulate the atmospheric environment of the ceramic method, the TG/DTG analysis of the pre-calcined raw precursor was carried out under CO(g) atmosphere (Fig. 2a). This analysis shows a 16 % mass loss starting around 900°C, which is related to the elimination of $CO_2(g)$ arising from $SrCO_3$ starting reagent. The asymmetric shape of the DTG curve (Fig. 2a) suggests a multistep decomposition in this temperature region. This thermal behavior can be a consequence of the exothermic formation of the materials' crystalline phase, which cannot be observed on the DTA curve (Fig. 2b) due to the endothermic decomposition in the same region. The energy released on the crystallization process may aid the endothermic decomposition, resulting in an initial fast decomposition observed on the TG curve [37]. Although the microwave heating implying a different decomposition pathway, the high temperature achieved in the MASS method (1350°C) was enough to result in a full decomposition of the carbonate precursors.

The FTIR absorption spectra of $Sr_2MgSi_2O_7:Eu^{2+},Dy^{3+}$ material prepared by MASS and ceramic methods are similar (SM Fig. S3), and the main peaks are described in the SM Table S2. The absorption peaks at 621 and 1008 cm^{-1} are assigned to the symmetric stretching of Si–O_B–Si and Si–O_T–Si (O_B: non-bridge oxygen and O_T: bridge oxygen) respectively [37,38]. These bands indicate that the $Sr_2MgSi_2O_7$ disilicate host is present in both synthetic methods. It is noteworthy that the CO_3^{2-} vibration bands (698, 857, 1086, and 1486 cm^{-1}) observed in the raw precursor are not present in the synthesized materials. This result confirms that the carbonate precursors have been decomposed in both synthesis processes.

The $Sr_2MgSi_2O_7$ host matrix has an *Åkermanite-type* $Ca_2MgSi_2O_7$ structure (Fig. 3) consisting of interconnected SiO_4 and MgO_4 tetrahedron sheets sharing an oxygen atom and held by eight coordinated Sr^{2+} interlayers with C_S low site symmetry [6,39,40]. The SiO_4 orthosilicate tetrahedrons are linked in pairs forming the Si_2O_7 pyrosilicate groups [39]. The SR-XPD patterns of the $Sr_2MgSi_2O_7:Eu^{2+},Dy^{3+}$ materials (Fig. 4) show the formation of the tetragonal phase ($P\bar{4}2_1m$ space group; No. 113; Z = 2) with a = b = 8.00771 Å, c = 5.17041 Å and $\alpha = 90^{\circ}$ lattice parameters (obtained in the Rietveld refinement for MASS method) [6]. The structural data indicate no major differences in

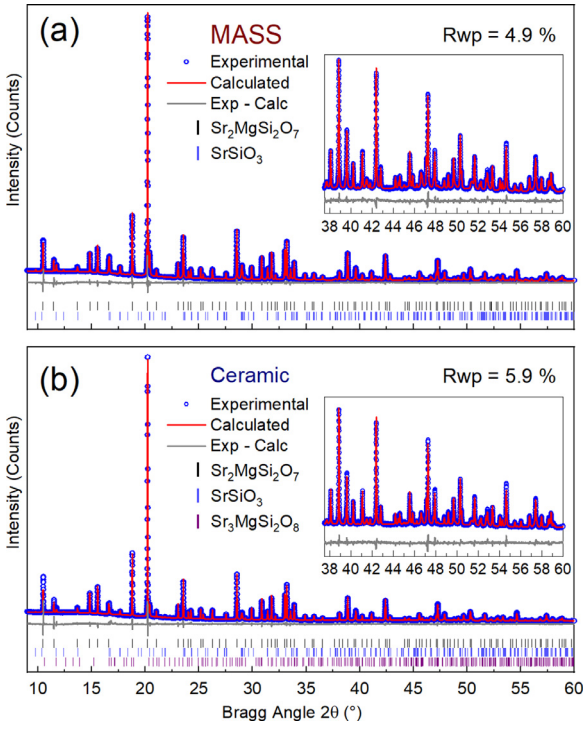

Fig. 4. Rietveld refinements of $Sr_2MgSi_2O_7:Eu^{2+},Dy^{3+}$ prepared by (a) MASS and (b) ceramic methods. In the inset, the low-intensity region shows a good agreement between experimental data and the calculated model. The vertical tick bars stand for: (black) $Sr_2MgSi_2O_7$, (blue) $SrSiO_3$ and (magenta) $Sr_3MgSi_2O_8$ (For interpretation of the references to color in this figure legend, the reader is referred to the web version of this article.).

the lattice parameters when compared with the data from their CIF Ref. [40].

Based on the Rietveld refinement, 14.7 % of the $SrSiO_3$ impurity phase was quantified on $Sr_2MgSi_2O_7$:Eu^{2+},Dy^{3+} material prepared by the MASS method. Furthermore, 9.7 and 0.4 % of $SrSiO_3$ and $Sr_3MgSi_2O_8$ phases were respectively determined to the material prepared by the ceramic method. Since vacancies are expected, especially for Sr, Mg, and O species, their occupations were refined. Considering that the O^{2-} and Mg^{2+} ions are too small for a precise calculation, the result was obtained as the mean occupation between Sr sites (SM Table S3). Although the light elements (such as O) are best probed using other techniques such as neutron scattering, the reliability of the Rietveld refinement is confirmed by a good agreement between the experimental data and the calculated model (Rwp < 10%) [42–44].

The remarkable match between Eu^{2+} (1.25 Å, CN:8) and Sr^{2+} (1.26 Å, CN:8) ionic radii confers a substitution without considerable lattice distortions. On the other hand, the ionic radii difference between Dy^{3+} (1.027 Å, CN: 8) and Sr^{2+} (1.26 Å, CN:8) is higher than the limit of solid solubility given by *Vegard's law* (size difference <15%). However, the low doping concentration provides a suitable substitution for these species. The Dy^{3+} charge compensation in this material creates defects such as interstitial O^{2-} and, more probably, the Sr^{2+} vacancies which are represented by *Kröger–Vink* notation in the Eqs. (1) and (2): [6,36,45]

$$Dy_2O_3 \xrightarrow{Sr_2MgSi_2O_7} 2Dy_{Sr}^{\cdot} + 2O_O^{\times} + O_i'' \quad (1)$$

$$Dy_2O_3 \xrightarrow{Sr_2MgSi_2O_7} 2Dy_{Sr}^{\cdot} + 3O_O^{\times} + V_{Sr}'' \quad (2)$$

where V_{Sr}'' represents Sr^{2+} vacancies and O_i'' interstitial O^{2-} ions. Moreover, intrinsic defects are expected at high-temperature syntheses such as *Schottky* defects caused by SrO and MgO volatilizations, leading to Sr^{2+}, Mg^{2+}, and O^{2-} vacancies. Duan *et al.* showed by DFT calculations that Mg^{2+} vacancies are more probable to occur than the Sr^{2+} ones. In this case, despites the higher bonding energy of Mg–O compared with Sr–O, the eight-fold coordination of strontium (SrO_8) implies in more energy to remove a Sr^{2+} ion from eight surrounding O^{2-} ligands than a Mg^{2+} ion from only four in a tetrahedrally coordinated site (MgO_4) [46]. The positive oxygen vacancies ($V_O^{\cdot\cdot}$) are particularly interesting due to its capacity to act as an electron trap energetically close to the bottom of the conduction band (CB). The $V_O^{\cdot\cdot}$ *Schottky* pair formation is an endothermic reaction with positive entropy variation, once the breaking of Sr–O, Mg–O, and Si–O bonds is not compensated by the formation of the gaseous oxides. Thus, the use of high temperature favors the thermodynamics of this process, especially when combined with reducing atmospheres. The very slow vacancy formation kinetics leads to long annealing periods when classical heating methods are used. In this context, the MASS preparation method presents as an innovation methodology due to the influence of the electrical field of the microwaves on the material, making possible the reduction of synthesis time.

Another essential parameter of persistent luminescent materials is the particle size, mainly because it can cause influences on the electronic and structural properties of these materials, such as their bandgap energy, spectroscopic behavior, and superficial defect distribution [12]. Using a powerful technique of frame-by-frame video-recording (SM Video S1), called Nanoparticle Tracking Analysis (NTA), it is possible to identify specific particle sizes and statistically create the cumulative size distribution (D_{10}, D_{50}, and D_{90}) of the powder samples with high precision. The NTA measurements of $Sr_2MgSi_2O_7$:Eu^{2+},Dy^{3+} material prepared by MASS and ceramic methods were carried out in dynamic conditions to avoid decantation artifacts and to allow the most extensive range of collected sample size, creating better statistic data (Fig. 5a,b).

Considering the raw precursors used in the MASS and ceramic methods as the same mixture of metal oxides and carbonates, the morphological properties differences will only depend on the thermal treatment used on each methodology. Taking into account that the powder samples were treated at high temperatures, in a resistive furnace as well as *via*

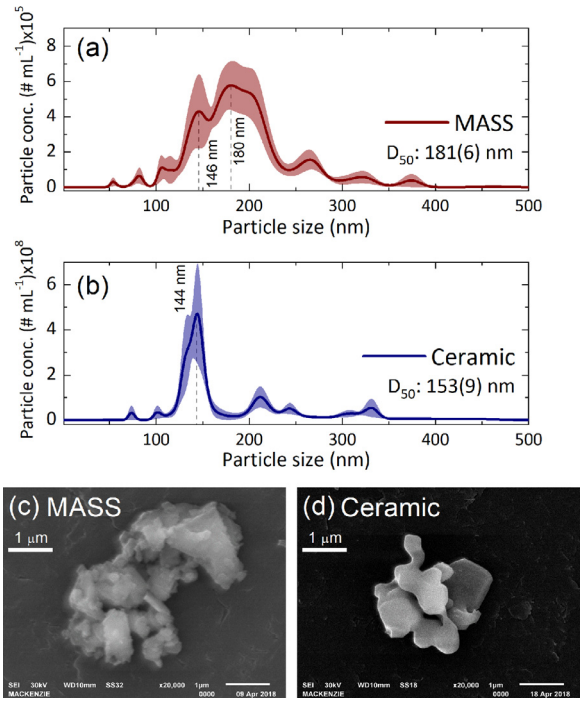

Fig. 5. NTA particle-size distribution (a,b) and SEM morphological analyses (c,d) of the $Sr_2MgSi_2O_7$:Eu^{2+},Dy^{3+} materials obtained *via* MASS and Ceramic methods, respectively.

microwave-assisted heating, particles with bigger sizes are commonly formed, whether agglomerates or even aggregates, as can be observed in SEM images (Fig. 5c,d).

The NTA curve shows the narrow distribution shape of the material prepared by the ceramic method (Fig. 5a), indicating that the long annealing period (5 h) at high temperature (1150°C) yields to the uniformization of particles sizes, with the D_{50} fraction value corresponding to 153 nm. This result indicates the well-sintered particles due to a long time of ceramic synthesis, confirmed by the SEM images (Fig. 5c).

However, the NTA curve of the material prepared by the MASS method shows a large particle size distribution with D_{50} = 181 nm (Fig. 5b). It also shows that larger particles are formed with the MASS method. In this case, the heating rate and rapid synthesis time do not allow the homogenization of particle sizes, and as shown in SEM images (Fig. 5d), the particles keep the plaque-like shape morphology characteristic of the carbonate precursors.

3.2. Europium valence and spectroscopic properties

The persistent luminescence mechanism of $Sr_2MgSi_2O_7$:Eu^{2+},Dy^{3+} material depends on the trapping of excited electrons from the divalent europium activator ion. Thus, the concentration of the Eu^{2+} ion can directly affect the persistent luminescence properties, increasing the duration of light-emitting after ceasing the excitation source. Therefore, the X-ray absorption near edge structure (XANES) spectroscopy was used to determine the qualitative proportion between the different Eu oxidation states. The XANES spectra of $Sr_2MgSi_2O_7$:Eu^{2+},Dy^{3+} material prepared by MASS and ceramic methods (Fig. 6) exhibit two absorption peaks centered at 6975 and 6984 eV assigned to the Eu^{2+} and Eu^{3+} L_{III} edges, respectively [47]. The $A_{(2+/3+)}$ reduction parameter is determined by the ratio between the areas under the curves in their absorption spectra (Fig. 6). These results indicate that both divalent and trivalent species are present in the material prepared by MASS and ceramic methods.

As can be seen from the XANES spectrum of the material prepared by the ceramic method (Fig. 6b), the Eu^{3+} absorption band area is bigger than that to the Eu^{2+} ion ($A_{(2+/3+)}$ = 0.66). This result indicates that the

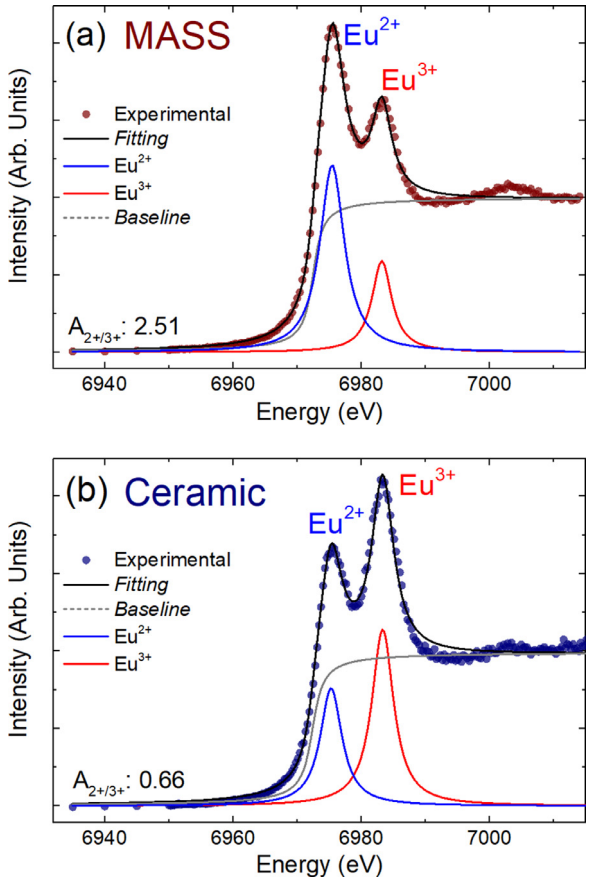

Fig. 6. X-ray absorption spectra in the XANES region of the $Sr_2MgSi_2O_7$:Eu^{2+},Dy^{3+} material prepared by (a) MASS and (b) ceramic methods. The ratio of divalent and trivalent europium species ($A_{2+/3+}$) was calculated from the deconvoluted curves using the integrated area of their respective peaks.

trivalent europium concentration is dominant for the material synthesized in the conventional furnace. Since the ceramic method requires a long time to be completed, the Eu^{2+} re-oxidation phenomenon may take place, probably because the CO(g) atmosphere is not continuously generated by activated charcoal, during the whole process. The reduction of CO(g) concentration is critical during the cooling process, once the CO(g) formation decays with the decreasing temperature [48,49]. Considering that the thermal inertia of resistive furnace is higher than the microwave oven, this process may be most prominent in the ceramic method. Besides, the CO(g) atmosphere reduces mostly the surfaces of the material, while the inner remains with a considerable amount of Eu^{3+} species.

Differently, the MASS route using microwave dielectric heating induces a rapid formation of material where the CO(g) atmosphere is generated during the whole process, which keeps the Eu^{2+} species stable leading to a higher reduction ratio $A_{(2+/3+)} = 2.51$ (Fig. 6a). Also, microwave radiation can increase the CO(g) conversion from the activated charcoal [48] and also induces the enhancement of ionic diffusion rate through the material, bringing the Eu^{3+} ions to the surface, thus improving the reducing process [50]. Therefore, considering these effects and the higher temperature achieved on the microwave oven, the MASS method is more efficient in producing Eu^{2+} species in $Sr_2MgSi_2O_7$:Eu^{2+},Dy^{3+} compared to the conventional ceramic method.

Another advantage of the X-ray absorption technique is the possibility to realize the *in-situ* measurements during the chemical reaction, allowing the study of the $Eu^{3+} + e^- \rightarrow Eu^{2+}$ reduction process in the material synthesis. Therefore, the *in-situ* XANES spectra were recorded through monitoring the Eu L_{III} edge during the heating of the precalcined raw precursor under He:CO (95:5 %) atmosphere (Fig. 7a). The *in-situ* XANES spectra carried out in the temperature interval from 30 to 800°C show only the absorption peak at 6984 eV assigned to the Eu^{3+} ion. Above 800°C, the absorption peak at 6978 eV is observed indicating the start of the $Eu^{3+} \rightarrow Eu^{2+}$ reduction process. This *in-situ* analysis reveals that the reduction process increases with the temperature rising from 800 to 1150°C.

Moreover, monitoring the Eu^{2+} absorption peak evolution at 6978 eV gives information about the reduction process during the material synthesis (Fig. 7b, green line). The derivative curve (Fig. 7b, black line) shows an increase of reduction rate with the maximum at 920°C, leading to a decreasing rate up to 1000°C. Despite the changing of CO(g) concentration which can barely affect the thermal behavior observed in the TG/DTA analysis, it is possible to correlate the increase of reduction with the decomposition of $SrCO_3$ around this temperature (Fig. 2a). The carbonate decomposition releases CO_2(g), hindering the interaction of Eu^{3+} ions with CO(g) atmosphere. According to TG data (Fig. 2a), the strontium carbonate decomposition process is completed at 1000°C, where is observed reduction rate stabilization up to 1020°C. After 1110°C, the reduction rate becomes insignificant, suggesting that the Eu^{2+} formation equilibrium has been reached.

The excitation spectra of the $Sr_2MgSi_2O_7$:Eu^{2+},Dy^{3+} material prepared by MASS and ceramic methods (Fig. 8a) present four broad absorption bands convoluted in the region from 275 to 470 nm, assigned to Eu^{2+} $4f^7(^8S_{7/2}) \rightarrow 4f^6 5d^1$ transitions. The excitation band in the visible range from 400 to 470 nm is of technological interest since it allows the persistent luminescence materials to be excited with sunlight and conventional blue LEDs. It is worth noting that the excitation spectra were collected monitoring the emission wavelength at 520 nm, aiming to record the full profile of the excitation band (275 – 460 nm) with no influence of the incident light source.

The emission spectra of the materials (Fig. 8b) show a broadband (430 to 550 nm) centered in 470 nm assigned to $4f^6 5d^1 \rightarrow 4f^7(^8S_{7/2})$ transition of the Eu^{2+} ion. Moreover, the low intensity peaks at 613 nm are assigned to the hypersensitive $^5D_0 \rightarrow ^7F_2$ transition of the Eu^{3+} ion (Fig. 8b, inset). The lowest emission intensity of this intraconfigurational of the material prepared by the MASS method indicates a more efficient $Eu^{3+} \rightarrow Eu^{2+}$ reduction, which is corroborated by XANES data (Fig. 6).

The bandgap energy information of the material was obtained by synchrotron radiation in the vacuum-UV region. The VUV excitation spectra (Fig. 8c) show one absorption band at 5.4 eV, which corresponds to the Eu^{2+} $4f^7(^8S_{7/2}) \rightarrow 4f^6 5d^1$ transitions. The highest intensity absorption band centered at 7.1 eV is assigned to the transition from the valence band, composed mainly by O (2p), Si (3p), and Sr (4p) orbitals of the host, to unoccupied Sr (4d) orbitals of the conduction band [6,51,52]. The bandgap energies of material prepared by MASS and ceramic methods were determined by the derivative method from the absorption curves, resulting in the equivalent value of 6.9 ± 0.1 eV (Fig. 8c) [9].

It is noteworthy that after UV irradiation, the excited electron can be stored in the host lattice defects, such as $V_{\ddot{O}}$, or into the Dy^{3+} cations, temporarily creating Dy^{2+} as recently proven by Joos et al. [53]. The charge carrier transfer from traps to the conduction band is governed by thermal energy (kT). Thus, thermoluminescence measurements are generally used to determine the defects energy levels and their concentrations. Although the TL intensity depends on the defect concentrations, accurate measurements of traps in terms of energy is a tough task, which will not be addressed in this work [54]. Besides, the TL intensity mainly shows the activated trap concentrations, *i.e.*, the traps that received a charge carrier from an emitting center. It means that even the material with plenty of traps, but without enought emitting centers, can still exhibit very low-intensity TL glow curves. Our material was prepared with the same amount of Dy^{3+}, which acts as the main trap. The TL glow curves (Fig. 8d) exhibit an intense emission band around 100°C, which

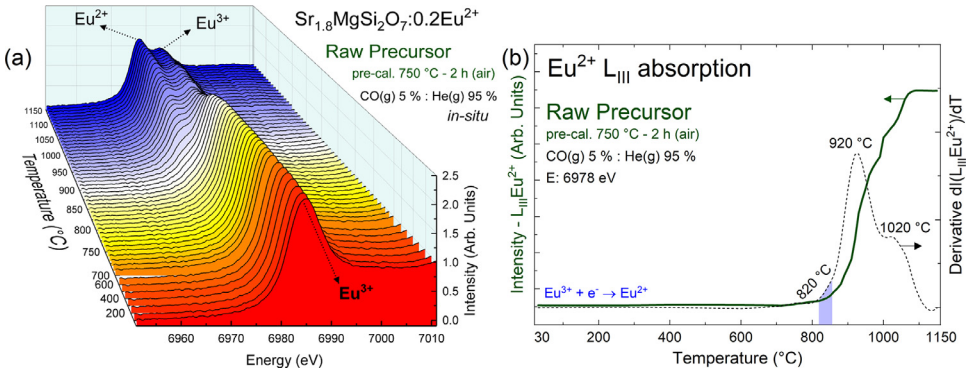

Fig. 7. (a) *In-situ* X-ray absorption spectra in the XANES region of the $Sr_{1.8}MgSi_2O_7$:0.2Eu^{2+} raw precursor in the function of the temperature under He:CO 95:5 % atmosphere and (b) evolution of Eu^{2+}-L_{III} edge absorption peak intensity (6986 eV).

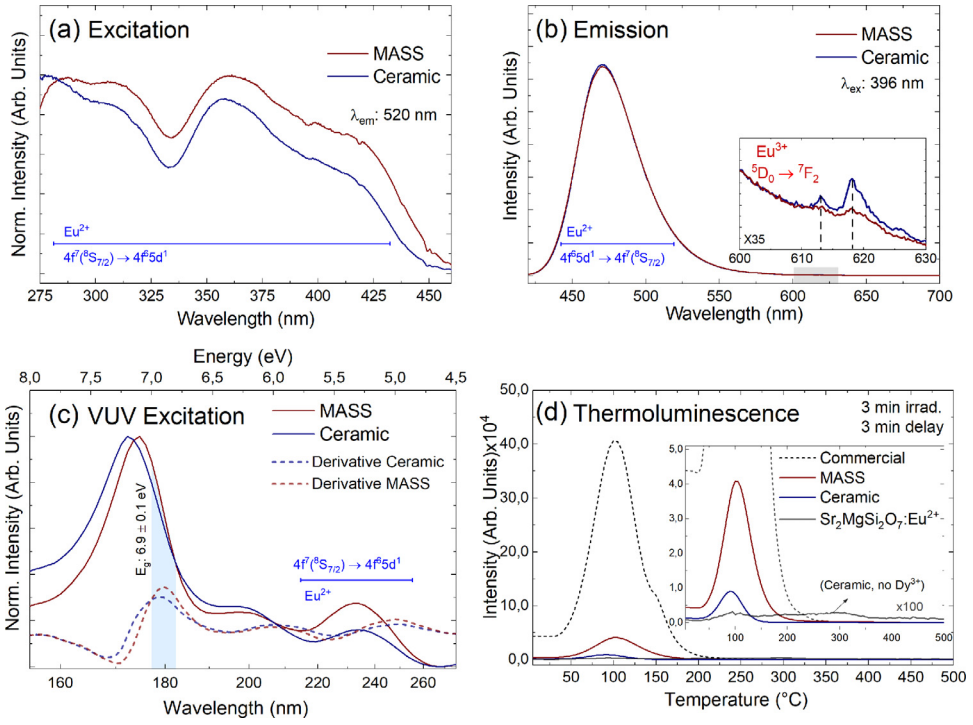

Fig. 8. Luminescence analyses of the $Sr_2MgSi_2O_7$:Eu^{2+},Dy^{3+} material prepared by MASS and ceramic methods: (a) excitation, (b) emission, and (c) VUV synchrotron radiation excitation spectra, and (d) thermoluminescence (TL) glow curves.

is often observed in the most efficient persistent luminescent materials reported in the literature [2,22,34,36,37,55–65].

The material obtained with the MASS method exhibits higher intensity at this optimal region than the glow curve of ceramic method material, suggesting a higher concentration of activated traps with low energy (shallow defects) involved in the emission process. Considering the persistent luminescence spectra registered through 5 min after ceasing the irradiation (SM Fig. S4), the same $4f^65d^1 \rightarrow 4f^7(^8S_{7/2})$ band is observed with no differences during the decay, indicating that only the Eu^{2+} ion acts as the emitter ion on persistent luminescence mechanism. Moreover, comparing the Dy-codoped and the $Sr_2MgSi_2O_7$:Eu^{2+} materials is possible to conclude that the major contribution of the trapping mechanism comes from Dy^{3+} ions.

Since Dy^{3+} nominal concentration is the same in all samples, the highest TL intensity (and consequently longest persistent luminescence decay time) is not governed only by this type of defect concentration. The amount of emitting centers *i.e.* the reduced Eu^{2+} species is the main responsible for populating the traps, which are probably not fully activated in ceramic prepared material.

Several features must be considered to the persistent luminescence decay time, for example, the purity of the material, particle size, or even the formation of dopant clusters. Fig. 9a shows the persistent luminescence decay times of the material prepared by MASS and ceramic methods. Despite the persistent luminescence decay time *via* luminance measurements is recommended, the comparison between the materials is possible using the high efficient commercial $Sr_2MgSi_2O_7$:Eu^{2+},Dy^{3+} sample (Yada Luminescent Co. Ltd., YD-#7506) as a benchmark. It is possible to observe that the material prepared by the MASS method exhibits higher emission intensity compared to that prepared by the ceramic method (~100 times) in the persistent luminescence decay time interval up to 120 min. Considering that the electron trapping/detrapping process depends mainly on the dopant Eu^{2+} emitter center and co-dopant Dy^{3+} trap, it is expected that the persistent luminescence phenomenon will be strongly affected by effects induced by the preparation method. The higher reduction process efficiency of Eu^{3+} ions provided by the MASS method results in more Eu^{2+} emitter species, which is confirmed by the XANES analysis (Fig. 6). Therefore, a higher divalent europium concentration may corroborate with the improvement of the persistent luminescence emission duration time. Besides, it was demonstrated by TL curves (Fig. 8d) that this material also presents a higher concentration of activated traps arising from the Dy^{3+} ion, which contributes to an increasing of the persistent luminescence emission time. These features lead to a longer persistent luminescence decay time (Fig. 9a) for the MASS material.

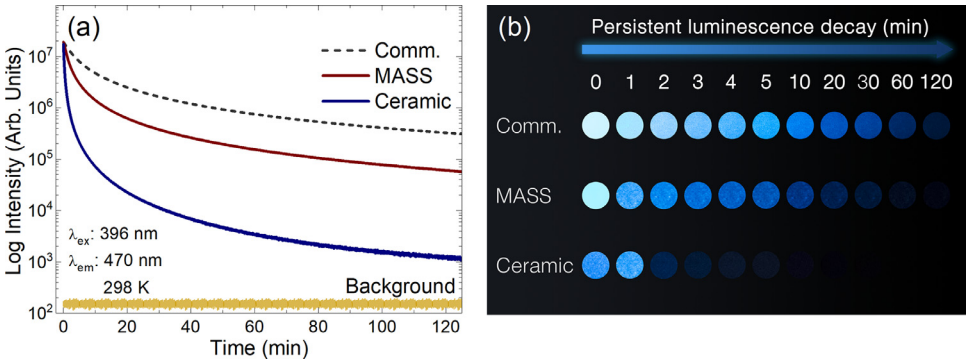

Fig. 9. (a) Decay time glow curves of $Sr_2MgSi_2O_7$:Eu^{2+},Dy^{3+} prepared by MASS and ceramic methods and their correspondent commercial material (Yada Luminescent Co. Ltd., YD-#7506) excited with 396 nm and monitored at 470 nm and (b) photographs of all samples taken using a digital camera to show the blue persistent luminescence emissions after 3 min of irradiation with 365 nm UV lamp.

The optical behavior of the material prepared *via* MASS and ceramic methods can be compared to its commercial reference as visualized in Fig. 9b. The blue emission was confirmed by the persistent luminescence emission spectra (SM Fig. S4). Finally, the microwave-assisted solid-state synthesis was considered an efficient substitute to prepare the well-established $Sr_2MgSi_2O_7$:Eu^{2+},Dy^{3+} with high efficient persistent luminescence.

4. Conclusion

The $Sr_2MgSi_2O_7$:Eu^{2+},Dy^{3+} material was successfully prepared by the single-step MASS method using microwave dielectric heating, leading to considerable advantages, such as rapid synthesis (less than 5 % of ceramic synthesis time), low-cost infrastructure, energy-saving approach, and improvement of optical properties of final product.

Furthermore, a significant enhancement of Eu^{2+} concentration in the host matrix was achieved by the MASS method, due to the CO(g) local atmosphere generation and faster ionic diffusion rate promoted by the microwave radiation interaction.

The *in-situ* XANES analysis elucidated the temperature dependence of the $Eu^{3+} \rightarrow Eu^{2+}$ reduction, showing that this process starts mainly above 900°C, influenced by the thermal decomposition of the raw precursor. The presence of the Eu^{2+} species in the host matrix is pivotal due to its charge donner role in the energy storage of the persistent luminescence phenomenon.

Moreover, the increase of the TL emission band at 100°C in the material prepared by the MASS method indicates a higher concentration of activated traps, due to the presence of Dy^{3+} ion that works on the improvement of persistent luminescence duration at room temperature.

The excitation spectra show a broad absorption band from UV to visible range (from 220 to 450 nm), which is crucial to development of new solar radiation harvesting energy technologies. The emission spectra show a broadband centered in the blue region (λ_{ex} = 470 nm) assigned to Eu^{2+} $4f^65d^1 \rightarrow 4f^7(^8S_{7/2})$ transitions. Therefore, the material prepared by the MASS method showed a strong enhancement of persistent luminescence duration time, corroborating with XANES and TL results. Lastly, microwave-assisted solid-state synthesis could be turned into a fast and efficient single-step way to prepare high-quality persistent luminescence materials for applications as emergency signs, anti-counterfeiting markers, and solar cell sensitizers.

Supplementary materials

Additional details of the heating setup of ceramic and MASS methods, as well as basic characterization of the $Sr_2MgSi_2O_7$:Eu^{2+},Dy^{3+} materials can be viewed in the Supplementary material.

Data availability

The raw/processed data required to reproduce these findings cannot be shared at this time as the data also forms part of an ongoing study.

Declaration of Competing Interest

The authors declare that they have no known competing financial interests or personal relationships that could have appeared to influence the work reported in this paper.

Acknowledgment

Funding: This work was supported by: (grant #2019/21770-5 and #2018/05280-5), São Paulo Research Foundation (FAPESP); (grant #427733/2016-2 and #427312/2016-7), National Council for Scientific and Technological Development (CNPq); (grant PROEX 3300201019P0), Coordination for the Improvement of Higher Education Personnel (CAPES). The authors would like to thank the following collaborators: Prof. Dr. Jorge A.S. Tenório, Dr. Victor B. Telles, and Dr. Jorge L. Coleti for the TG-DTA analysis; Abner Cabral Neto from Mackenzie University (Higienópolis campus, São Paulo – SP) for the SEM images; MSc. Junior C. Maurício, Dr. Anna P.S.S. Levinsky and Dr. Santiago Figueroa for the XAFS2 beamline supporting (#20170006); Dr. Alexey Marques Espíndola and Dr. Amelie Claire Rochet for DXAS beamline measurements (#20180094); Dr. Douglas Galante and Eng. Leonardo Kofukuda for TGM beamline measurements (#20170461); Eng. Douglas Henrique Araujo for XRD1 supporting (#20170861); Dr. Adriana Franco Paes Leme and Dr. Sami Yokoo from LNBio-CNPEM (grant #2010/19278-0, FAPESP) for NTA analyses.

Supplementary materials

Supplementary material associated with this article can be found, in the online version, at doi:10.1016/j.mtla.2021.101226.

References

[1] P. Dorenbos, Mechanism of persistent luminescence in $Sr_2MgSi_2O_7$:Eu^{2+}; Dy^{3+}, Phys. Status Solidi. 242 (2005) R7–R9, doi:10.1002/pssb.200409080.
[2] K. Van den Eeckhout, P.F. Smet, D. Poelman, Persistent luminescence in Eu^{2+}-doped compounds: a review, Materials 3 (2010) 2536–2566 (Basel), doi:10.3390/ma3042536.
[3] M. Lastusaari, T. Laamanen, M. Malkamäki, K.O. Eskola, A. Kotlov, S. Carlson, E. Welter, H.F. Brito, M. Bettinelli, H. Jungner, J. Hölsä, The bologna stone: history's first persistent luminescent material, Eur. J. Mineral. 24 (2012) 885–890, doi:10.1127/0935-1221/2012/0024-2224.
[4] J. Hölsä, Persistent luminescence beats the afterglow: 400 years of persistent luminescence, Electrochem. Soc. Interface 4 (2009) 42–45 http://www.electrochem.org/dl/interface/wtr/wtr09/wtr09_p042-045.pdf, doi:10.1149/2.F06094IF.
[5] J. Hölsä, T. Laamanen, M. Lastusaari, M. Malkamäki, P. Novák, Persistent luminescence - Quo vadis? J. Lumin. 129 (2009) 1606–1609, doi:10.1016/j.jlumin.2008.12.027.
[6] M. Lastusaari, H. Jungner, A. Kotlov, T. Laamanen, L.C.V. Rodrigues, H.F. Brito, J. Hölsä, Understanding persistent luminescence: rare-earth- and Eu^{2+}-doped $Sr_2MgSi_2O_7$, Zeitschrift Für Naturforsch. B. 69 (2014) 171–182, doi:10.5560/znb.2014-3322.
[7] H.F. Brito, J. Hölsä, T. Laamanen, M. Lastusaari, M. Malkamäki, L.C.V. Rodrigues, Persistent luminescence mechanisms: human imagination at work, Opt. Mater. Express. 2 (2012) 371, doi:10.1364/OME.2.000371.

[8] C. Zhao, D. Chen, Synthesis of $CaAl_2O_4$:Eu,Nd long persistent phosphor by combustion processes and its optical properties, Mater. Lett. 61 (2007) 3673–3675, doi:10.1016/j.matlet.2006.12.015.

[9] T. Aitasalo, J. Hassinen, J. Hölsä, T. Laamanen, M. Lastusaari, M. Malkamäki, J. Niittykoski, P. Novák, Synchrotron radiation investigations of the $Sr_2MgSi_2O_7$:Eu^{2+},R^{3+} persistent luminescence materials, J. Rare Earths. 27 (2009) 529–538, doi:10.1016/S1002-0721(08)60283-5.

[10] Z. Pan, Y.Y. Lu, F. Liu, Sunlight-activated long-persistent luminescence in the near-infrared from Cr^{3+}-doped zinc gallogermanates, Nat. Mater. 11 (2012) 58–63, doi:10.1038/nmat3173.

[11] M. Suta, C. Wickleder, Synthesis, spectroscopic properties and applications of divalent lanthanides apart from Eu^{2+}, J. Lumin. 210 (2019) 210–238, doi:10.1016/j.jlumin.2019.02.031.

[12] E. Bonturim, L.G. Merizio, R. dos Reis, H.F. Brito, L.C.V. Rodrigues, M.C.F.C. Felinto, Persistent luminescence of inorganic nanophosphors prepared by wet-chemical synthesis, J. Alloys Compd. 732 (2018) 705–715, doi:10.1016/j.jallcom.2017.10.219.

[13] K. Van den Eeckhout, D. Poelman, P. Smet, Persistent luminescence in Non-Eu^{2+}-doped compounds: a review, Materials 6 (2013) 2789–2818 (Basel), doi:10.3390/ma6072789.

[14] C.C.S. Pedroso, J.M. Carvalho, L.C.V. Rodrigues, J. Hölsä, H.F. Brito, Rapid and energy saving microwave-assisted solid-state synthesis of Pr^{3+}, Eu^{3+} or Tb^{3+} doped Lu_2O_3 persistent luminescence materials, ACS Appl. Mater. Interfaces 8 (2016) 19593–19604, doi:10.1021/acsami.6b04683.

[15] J. Miranda de Carvalho, C.C.S. Pedroso, I.P. Machado, J. Hölsä, L.C.V. Rodrigues, P. Głuchowski, M. Lastusaari, H.F. Brito, Persistent luminescence warm-light LEDs based on Ti-doped RE_2O_2S materials prepared by rapid and energy-saving microwave-assisted synthesis, J. Mater. Chem. C. 6 (2018) 8897–8905, doi:10.1039/C8TC01826J.

[16] S. Do Han, K.C. Singh, T.Y. Cho, H.S. Lee, D. Jakhar, J.P. Hulme, C.H. Han, J.D. Kim, I.S. Chun, J. Gwak, Preparation and characterization of long persistence strontium aluminate phosphor, J. Lumin. 128 (2008) 301–305, doi:10.1016/j.jlumin.2007.07.017.

[17] T. Aitasalo, P. Derén, J. Hölsä, H. Jungner, J.C. Krupa, M. Lastusaari, J. Legendziewicz, J. Niittykoski, W. Stręk, Persistent luminescence phenomena in materials doped with rare earth ions, J. Solid State Chem. (2003) 114–122, doi:10.1016/S0022-4596(02)00194-9.

[18] T. Maldiney, A. Bessière, J. Seguin, E. Teston, S.K. Sharma, B. Viana, A.J.J. Bos, P. Dorenbos, M. Bessodes, D. Gourier, D. Scherman, C. Richard, The *in vivo* activation of persistent nanophosphors for optical imaging of vascularization, tumours and grafted cells, Nat. Mater. 13 (2014) 418–426, doi:10.1038/nmat3908.

[19] H. Homayoni, L. Ma, J. Zhang, S.K. Sahi, L. Hossein, B. Bui, W. Chen, Photodiagnosis and photodynamic therapy synthesis and conjugation of $Sr_2MgSi_2O_7$:Eu^{2+},Dy^{3+} water soluble afterglow nanoparticles for photodynamic activation, Photodiagnos. Photodyn. Ther. 16 (2016) 90–99, doi:10.1016/j.pdpdt.2016.08.012.

[20] J. Hassinen, J. Hölsä, J. Niittykoski, T. Laamanen, M. Lastusaari, M. Malkamäki, P. Novák, UV-VUV spectroscopy of rare earth doped persistent luminescence materials, Opt. Mater. (Amst). 31 (2009) 1751–1754, doi:10.1016/j.optmat.2009.01.016.

[21] H. Wu, Y. Hu, Y. Wang, F. Kang, Z. Mou, Investigation on Eu^{3+} doped $Sr_2MgSi_2O_7$ red-emitting phosphors for white-light-emitting diodes, Opt. Laser Technol. 43 (2011) 1104–1110, doi:10.1016/j.optlastec.2011.02.006.

[22] T. Aitasalo, J. Hölsä, H. Jungner, M. Lastusaari, J. Niittykoski, Thermoluminescence study of persistent luminescence materials: Eu^{2+} - and R^{3+} -doped calcium aluminates, $CaAl_2O_4$:Eu^{2+},R^{3+}, J. Phys. Chem. B. 110 (2006) 4589–4598, doi:10.1021/jp057185m.

[23] H.F. Brito, J. Hassinen, J. Hölsä, H. Jungner, T. Laamanen, M. Lastusaari, M. Malkamäki, J. Niittykoski, P. Novák, L.C.V. Rodrigues, Optical energy storage properties of $Sr_2MgSi_2O_7$:Eu^{2+},R^{3+} persistent luminescence materials, J. Therm. Anal. Calorim. 105 (2011) 657–662, doi:10.1007/s10973-011-1403-2.

[24] H.J. Kitchen, S.R. Vallance, J.L. Kennedy, N. Tapia-Ruiz, L. Carassiti, A. Harrison, A.G. Whittaker, T.D. Drysdale, S.W. Kingman, D.H. Gregory, Modern microwave methods in solid-state inorganic materials chemistry: from fundamentals to manufacturing, Chem. Rev. 114 (2014) 1170–1206, doi:10.1021/cr4002353.

[25] E.E. Levin, J.H. Grebenkemper, T.M. Pollock, R. Seshadri, Protocols for high temperature assisted-microwave preparation of inorganic compounds, Chem. Mater. 31 (2019) 7151–7159, doi:10.1021/acs.chemmater.9b02594.

[26] K.J. Rao, B. Vaidhyanathan, M. Ganguli, P.A. Ramakrishnan, Synthesis of inorganic solids using microwaves, Chem. Mater. 11 (1999) 882–895, doi:10.1021/cm9803859.

[27] A.M.G. Carvalho, D.H.C. Araújo, H.F. Canova, C.B. Rodella, D.H. Barrett, S.L. Cuffini, R.N. Costa, R.S. Nunes, X-ray powder diffraction at the XRD1 beamline at LNLS, J. Synchrotron Radiat. 23 (2016) 1501–1506, doi:10.1107/S1600577516012686.

[28] A.M.G. Carvalho, R.S. Nunes, A.A. Coelho, X-ray powder diffraction of high-absorption materials at the XRD1 beamline off the best conditions: application to $(Gd,Nd)_5Si_4$ compounds, Powder Diffr. 32 (2017) 10–14, doi:10.1017/S0885715616000646.

[29] V. Filipe, A. Hawe, W. Jiskoot, Critical evaluation of nanoparticle tracking analysis (NTA) by NanoSight for the measurement of nanoparticles and protein aggregates, Pharm. Res. 27 (2010) 796–810, doi:10.1007/s11095-010-0073-2.

[30] S.J.A. Figueroa, J.C. Mauricio, J. Murari, D.B. Beniz, J.R. Piton, H.H. Slepicka, M.F. de Sousa, A.M. Espíndola, A.P.S. Levinsky, Upgrades to the XAFS2 beamline control system and to the endstation at the LNLS, J. Phys. Conf. Ser. 712 (2016) 012022, doi:10.1088/1742-6596/712/1/012022.

[31] H.C.N. Tolentino, J.C. Cezar, N. Watanabe, C. Piamonteze, N.M. Souza-Neto, E. Tamura, A.Y. Ramos, R. Neueschwander, The dispersive X-ray absorption spectroscopy beamline at LNLS, Phys. Scr. T115 (2005) 977, doi:10.1238/Physica.Topical.115a00977.

[32] R.L. Cavasso Filho, A.F. Lago, M.G.P. Homem, S. Pilling, A. Naves de Brito, Delivering high-purity vacuum ultraviolet photons at the Brazilian toroidal grating monochromator (TGM) beamline, J. Electron Spectros. Relat. Phenomena. 156–158 (2007) 168–171, doi:10.1016/j.elspec.2006.11.026.

[33] V.C. Teixeira, L.C.V. Rodrigues, D. Galante, M.V. dos S. Rezende, Effect of lithium excess on the $LiAl_5O_8$:Eu luminescent properties under VUV excitation, Opt. Mater. Express. 6 (2016) 2871, doi:10.1364/OME.6.002871.

[34] T. Aitasalo, J. Hölsä, M. Kirm, T. Laamanen, M. Lastusaari, J. Niittykoski, J. Raud, R. Valtonen, Persistent luminescence and synchrotron radiation study of the $Ca_2MgSi_2O_7$:Eu^{2+},R^{3+} materials, Radiat. Meas. 42 (2007) 644–647, doi:10.1016/j.radmeas.2007.01.058.

[35] I.P. Machado, V.C. Teixeira, C.C.S. Pedroso, H.F. Brito, L.C.V. Rodrigues, X-ray scintillator Gd_2O_2S:Tb^{3+} materials obtained by a rapid and cost-effective microwave-assisted solid-state synthesis, J. Alloys Compd. 777 (2019) 638–645, doi:10.1016/j.jallcom.2018.10.348.

[36] T. Aitasalo, J. Hölsä, T. Laamanen, M. Lastusaari, L. Lehto, J. Niittykoski, F. Pellé, Luminescence properties of Eu^{2+} doped dibarium magnesium disilicate, $Ba_2MgSi_2O_7$:Eu^{2+}, Ceram. Silikaty 49 (2005) 58–62.

[37] L. He, B. Jia, L. Che, W. Li, W. Sun, Preparation and optical properties of afterglow $Sr_2MgSi_2O_7$:Eu^{2+},Dy^{3+} electrospun nanofibers, J. Lumin. 172 (2016) 317–322, doi:10.1016/j.jlumin.2015.12.012.

[38] R. Shrivastava, J. Kaur, Characterisation and Mechanoluminescence studies of $Sr_2MgSi_2O_7$:Eu^{2+},Dy^{3+}, J. Radiat. Res. Appl. Sci. 8 (2015) 201–207, doi:10.1016/j.jrras.2015.01.005.

[39] M.A. Tshabalala, H.C. Swart, F.B. Dejene, E. Coetsee, O.M. Ntwaeaborwa, Structure, surface analysis, photoluminescent properties and decay characteristics of Tb^{3+}-Eu^{3+} co-activated $Sr_2MgSi_2O_7$ phosphor, Appl. Surf. Sci. 360 (2016) 409–418, doi:10.1016/j.apsusc.2015.10.200.

[40] M. Kimata, The structural properties of synthetic Sr-åkermanite, $Sr_2MgSi_2O_7$, Zeitschrift Für Krist. - Cryst. Mater. 163 (1983) 295–304, doi:10.1524/zkri.1983.163.3-4.295.

[41] K. Momma, F. Izumi, VESTA 3 for three-dimensional visualization of crystal, volumetric and morphology data, J. Appl. Crystallogr. 44 (2011) 1272–1276, doi:10.1107/S0021889811038970.

[42] B.H. Toby, R factors in Rietveld analysis: how good is good enough? Powder Diffr. 21 (2006) 67–70, doi:10.1154/1.2179804.

[43] E.B.V. Freire, A.L. de S. Santos, G.F. da C. Bispo, M. de A. Gomes, Z.S. Macedo, R.A. Jackson, M.E.G. Valerio, Intrinsic defects and non-stoichiometry in undoped cadmium silicate hosts, J. Alloys Compd. 857 (2021) 157580, doi:10.1016/j.jallcom.2020.157580.

[44] G.F.C. Bispo, A.B. Andrade, C. dos S Bezerra, V.C. Teixeira, D. Galante, M.E.G. Valerio, Luminescence in undoped CaYAl3O7 produced via the Pechini method, Phys. B Condens. Matter. 507 (2017) 119–130, doi:10.1016/j.physb.2016.12.002.

[45] H. Wu, Y. Hu, Y. Wang, C. Fu, The luminescent properties of the substitution of Ho^{3+} for Dy^{3+} in the $M_2MgSi_2O_7$: Eu^{2+}, Dy^{3+} (M: Sr, Ca) long afterglow phosphors, Mater. Sci. Eng. B. 172 (2010) 276–282, doi:10.1016/j.mseb.2010.05.030.

[46] H. Duan, Y.Z. Dong, Y. Huang, Y.H. Hu, X.S. Chen, First-principles study of intrinsic vacancy defects in $Sr_2MgSi_2O_7$ phosphorescent host material, J. Phys. D. Appl. Phys. 49 (2016) 025304, doi:10.1088/0022-3727/49/2/025304.

[47] J. Yan, C. Liu, J. Vlieland, J. Zhou, P. Dorenbos, Y. Huang, Y. Tao, H. Liang, Intense emission of $Ba_2MgSi_2O_7$:Eu^{2+} under X-ray excitation for potential detecting applications, J. Lumin. 183 (2017) 97–101, doi:10.1016/j.jlumin.2016.11.009.

[48] J. Hunt, A. Ferrari, A. Lita, M. Crosswhite, B. Ashley, A.E. Stiegman, Microwave-specific enhancement of the carbon–carbon dioxide (boudouard) reaction, J. Phys. Chem. C. 117 (2013) 26871–26880, doi:10.1021/jp4076965.

[49] P.J.R. Montes, V.C. Teixeira, D.A.B. Barbosa, C.W.A. Paschoal, M.V. dos S. Rezende, *In situ* investigation of Ba-substitution effect on the Eu^{3+}→Eu^{2+} conversion in SrAl2O4:Eu phosphor, J. Alloys Compd. 708 (2017) 79–83, doi:10.1016/j.jallcom.2017.02.299.

[50] A.G. Whittaker, Diffusion in microwave-heated ceramics, Chem. Mater. 17 (2005) 3426–3432, doi:10.1021/cm050351i.

[51] H. Duan, Y.Z. Dong, Y. Huang, Y.H. Hu, X.S. Chen, The important role of oxygen vacancies in $Sr_2MgSi_2O_7$ phosphor, Phys. Lett. A. 380 (2016) 1056–1062, doi:10.1016/j.physleta.2016.01.001.

[52] J. Hölsä, T. Laamanen, M. Lastusaari, P. Novák, Isolated defects in $Sr_2MgSi_2O_7$: a DFT study, Phys. Procedia. 29 (2012) 76–85, doi:10.1016/j.phpro.2012.03.701.

[53] J.J. Joos, K. Korthout, L. Amidani, P. Glatzel, D. Poelman, P.F. Smet, Identification of Dy^{3+}/Dy^{2+} as electron trap in persistent phosphors, Phys. Rev. Lett. 125 (2020) 033001, doi:10.1103/PhysRevLett.125.033001.

[54] K. Van den Eeckhout, A.J.J. Bos, D. Poelman, P.F. Smet, Revealing trap depth distributions in persistent phosphors, Phys. Rev. B 87 (2013) 045126, doi:10.1103/PhysRevB.87.045126.

[55] N. Suriyamurthy, B.S. Panigrahi, Effects of non-stoichiometry and substitution on photoluminescence and afterglow luminescence of $Sr_4Al_{14}O_{25}$:Eu^{2+},Dy^{3+} phosphor, J. Lumin. 128 (2008) 1809–1814, doi:10.1016/j.jlumin.2008.05.001.

[56] Z.X. Yuan, C. Chang, D.L. Mao, W. Ying, Effect of composition on the luminescent properties of $Sr_4Al_{14}O_{25}$: Eu^{2+}, Dy^{3+} phosphors, J. Alloys Compd. 377 (2004) 268–271, doi:10.1016/j.jallcom.2004.01.063.

[57] B. Liu, C. Shi, M. Yin, L. Dong, Z. Xiao, The trap states in the $Sr_2MgSi_2O_7$ and (Sr,Ca)$MgSi_2O_7$ long afterglow phosphor activated by Eu^{2+} and Dy^{3+}, J. Alloys Compd. 387 (2005) 65–69, doi:10.1016/j.jallcom.2004.06.061.

[58] T. Aitasalo, J. Hölsä, H. Jungner, J.C. Krupa, M. Lastusaari, J. Legendziewicz, J. Niittykoski, Effect of temperature on the luminescence processes of $SrAl_2O_4$:Eu^{2+}, Radiat. Meas. 38 (2004) 727–730, doi:10.1016/j.radmeas.2004.01.031.

[59] E. Nakazawa, T. Mochida, Traps in $SrAl_2O_4$:Eu^{2+} phosphor with rare-earth ion doping, J. Lumin. 72–74 (1997) 236–237, doi:10.1016/S0022-2313(97)00043-4.

[60] J. Du, O.Q. De Clercq, D. Poelman, Temperature dependent persistent luminescence: evaluating the optimum working temperature, Sci. Rep. 9 (2019) 10517, doi:10.1038/s41598-019-46889-z.
[61] H. Wu, Y. Hu, Y. Wang, Z. Mou, Influence on the long afterglow properties by the environmental temperature, J. Lumin. 130 (2010) 127–130, doi:10.1016/j.jlumin.2009.07.031.
[62] H. Wu, Y. Hu, Y. Wang, B. Zeng, Z. Mou, L. Deng, W. Xie, Influence on luminescent properties of the $Sr_2MgSi_2O_7$:Eu^{2+} by Dy^{3+}, Nd^{3+} co-doping, J. Alloys Compd. 486 (2009) 549–553, doi:10.1016/j.jallcom.2009.07.002.
[63] T. Matsuzawa, A new long phosphorescent phosphor with high brightness, $SrAl_2O_4$:Eu^{2+},Dy^{3+}, J. Electrochem. Soc. 143 (1996) 2670, doi:10.1149/1.1837067.
[64] E. Nakazawa, Y. Murazaki, S. Saito, Mechanism of the persistent phosphorescence in $Sr_4Al_{14}O_{25}$:Eu and $SrAl_2O_4$:Eu codoped with rare earth ions, J. Appl. Phys. 100 (2006) 113113, doi:10.1063/1.2397284.
[65] L. Jiang, C. Chang, D. Mao, B. Zhang, A new long persistent blue-emitting $Sr_2ZnSi_2O_7$:Eu^{2+}, Dy^{3+} prepared by sol–gel method, Mater. Lett. 58 (2004) 1825–1829, doi:10.1016/j.matlet.2003.11.014.